

# Strategic Scheduling of Discrete Control Devices in Active Distribution Systems

Alireza Nouri, *Member, IEEE*, Alireza Soroudi, *Senior Member, IEEE*, and Andrew Keane, *Senior Member, IEEE*

**Abstract**—The frequent actuation of discrete control devices (DCDS), e.g., on-load tap changers, drastically reduces their lifetime. This, in turn, imposes a huge replacement cost. Simultaneous scheduling of these DCDS and continuous control devices, e.g., distributed energy resources, is imperative for reducing the operating cost. This also increases the lifetime of DCDS and helps to avoid the sub-optimal/infeasible solutions. Considering the high cost of discrete control actions (DCAS), they may never be justified against the other options in a short scheduling horizon (SH). With a longer SH, their benefits over a long period justify DCAS. However, a shorter SH helps to hedge against the risk impelled by uncertainties. Here, the system future is modeled as a set of multi-period scenarios. The operator exploits a long SH, but solely applies the decisions made for the first period and waits for updated data to make the next decisions. This enables cost reduction by strategically applying DCAS prior to the time that they are inevitable, while avoiding them when unneeded. The proposed branch-and-cut-based solution methodology accurately deals with DCAS while applying some expediting heuristics. During the branching process, a globally convergent trust region algorithm solves the integer relaxed problems.

**Index Terms**—Active distribution systems, discrete control devices, OLTC, stochastic scheduling, static voltage control

## LIST OF ABBREVIATIONS

BC	Branch and cut
CB	Capacitor bank
DCA	Discrete controllable action
DCC	Discrete control cost
DCD	Discrete controllable device
DER	Distributed energy resource
DSP	Distribution scheduling problem
LP	Linear programming
MILP	Mixed integer linear programming
MINLP	Mixed integer nonlinear programming
NLP	Nonlinear programming
OC	Operation cost
OLTC	On load tap changer
PDF	Probability density function
RES	Renewable energy sources
RHC	Receding horizon control
SH	Scheduling horizon
SOCP	Second-order cone programming
SVR	Static voltage regulator
SA	Solution approaches

A. Nouri (alireza.nouri@ucd.ie), A. Soroudi (alireza.soroudi@ucd.ie) and A. Keane (andrew.keane@ucd.ie) are with the School of Electrical and Electronic Engineering, University College Dublin, Dublin 04, Ireland.

This work has emanated from research conducted with the financial support of Science Foundation Ireland under the SFI Strategic Partnership Programme Grant Number SFI/15/SPP/E3125. The opinions, findings and conclusions or recommendations expressed in this material are those of the authors and do not necessarily reflect the views of the Science Foundation Ireland.

TRA Trust region algorithm

## I. INTRODUCTION

WITH the increasing penetration of highly variable renewable production in active distribution systems, the resource scheduling and voltage control problem is increasingly becoming dynamic in nature. The variability of load levels and upstream system characteristics give rise to this issue. Discrete control devices (DCDS), e.g., on load tap changers (OLTCs) and capacitor banks (CBs), are able to control the voltage levels in the steady state conditions. However, maintaining the voltage levels within the predefined limits with only conventional DCDS entails frequent actuation of these devices. This reduces their lifetime. Due to their high cost, discrete control actions (DCAS), cannot be applied frequently. The use of DCDS should be optimally balanced with continuously controllable devices, e.g., distributed energy resources (DERS). In a short scheduling horizon (SH), DCAS may never be justified against the cheaper changes in active and reactive power supports of the continuous control devices. Therefore, they would never be applied unless they are inevitable. With a longer SH, their higher impact on operating cost reduction may justify these actions. In previous studies, DCAS were usually scheduled prior to the real-time operation, e.g., in a day-ahead period [1]. Conversely, to reduce the effects of uncertainties and to keep the solution optimality, the SH should be as short as possible. Therefore, each short and long SH has its own cons and pros.

Here, the term “Discrete Control Devices” is referred to a family of equipment and devices with a discrete controllable parameter. The main focus is on the co-optimization of the schedule of discrete and continuous control devices and steady state voltage control. To this end, the system future is modeled as a set of scenarios. Each scenario includes load levels, load characteristics, production levels of renewable energy sources (RESS), upstream system characteristics and utility prices, all in successive periods of the SH. In the first period, the same decisions are taken for all scenarios. Only the decisions taken for this period are implemented. The framework will be applied again to find the optimal schedule of the next periods. In this way, the decision maker benefits a long SH, makes the decisions based on the available and forecast data and waits for more accurate data to make the next decisions. Some DCAS are inevitable in the upcoming periods. Using the proposed method, the operator may be able to reduce the cost by applying these DCAS in advance. Since only the decisions of the first period are applied, the effects of uncertainties are also restricted.

The proposed solution methodology based on branch and cut (BC) technique accurately deals with the discrete control variables. This helps to avoid infeasibility/sub-optimality. During the branching process of branch and cut technique, an integer relaxed problem with additional bounds on integer variables should be solved at each node. A globally convergent trust region algorithm (TRA) is applied to solve these integer relaxed problems. The TRA sub-problems are solved using interior point method [2]. The details of the proposed solution methodology are provided in subsection II-B. The proposed method incorporates the accurate models and does not rely on simplifying assumptions such as those made in convex relaxation approaches, e.g., balanced operation (see I-A). Upstream system, OLTC, CBS and voltage dependent loads are accurately modeled. These models are kept up-to-date while solving the distribution scheduling problem (DSP).

### A. Literature Review

A multi-timescale coordinated control was proposed [1] and [3]. The system uncertainties were considered in the day-ahead scheduling of DCSS. However, there is still no guarantee that the fast (continuous) control devices can maintain the voltages within the limits in the intra-day scheduling problems. Moreover, during the next day, the operator is able to further reduce the system cost by readjusting the schedule of the DCDS based on the uncertainties already revealed. The main focus of [4] was on presenting a comprehensive framework for uncertainty handling in an unbalanced three-phase system based on information gap decision theory. A day-ahead scheduling was solved for DCAs. In this paper, the schedule of DCAs is changed according to as much data as available in the real-time operation and the latest forecast on the uncertain parameters based on receding horizon control (RHC). Tap-changing cost was modeled in [5]. The same model is used in this paper.

RHC technique was implemented in distribution systems to achieve different goals. This technique deals with the constrained dynamic optimization problems by finding a set of consecutive control actions derived by optimizing the objective function over a horizon window. RHC was applied in [6] to find the optimal set-points of DERs, in [7] to deal with the dynamics of energy storage systems and in [8] to schedule the deferrable loads. DCDS were not included in these studies. The ability of RHC technique to solve the issues related to the scheduling of DCDS has not yet been analyzed. With this technique employed to address the aforementioned issues of DCDS in AC DSP, computational burden at each time step can be deemed as a downside. The proposed method exploits the RHC technique to handle the DCDS and continuous control devices simultaneously. The computational burden is dealt with the solution methodology proposed in subsection II-B.

It was shown in [9] how the energy storage systems and demand response programs mitigate the effects of uncertainties. The main focus was on the planning of the battery storage systems and the DCDS were neglected. The operation sub-problems were also solved to achieve the feasible and optimal solutions. The storage systems can also be modeled in the formulation proposed in the present paper based on [7] and considering the practical requirements presented in [9]. Most

demand response programs and reliability measures cannot be modeled in a short SH. The proposed RHC-based scheduling can also be applied to handle these programs. The practical consideration of demand response programs and reliability concerns were discussed in [10] and [11], respectively.

The DSP is a MINLP problem that takes a long time to converge to a reliable solution. The uncertainties escalates the issue. Some previous works applied simplified formulations, e.g., linearized formulations [12], and also simplified models for DCDS, e.g., round-off approaches [13]. There is no guarantee that the solution is optimal or even feasible with these methods.

The state-of-the-art second order cone programming (SOCP) and the semidefinite programming based on branch flow model [14] have gained popularity in recent years. These methods are able to effectively solve the DSP in balanced active distribution systems enabled with continuous control devices under quite acceptable assumptions [15]. SOCP was applied in [16] to solve the stochastic day-ahead DSP. DCDS, e.g., OLTCs and CBS, was also taken into account. In order to model OLTC transformers, it was assumed that the primary voltage is fixed to avoid the non-linearity introduced by the discrete-linear product terms of turn ratio and primary voltage. The effects of bus voltage on the reactive power injected by CBS was also neglected for the same reason. Additional binary and continuous variables were introduced in [17] to present a linearized model for OLTCs. CBS can be modeled in the same way. For a long SH (which is inevitable with DCDS), the number of binary variables will drastically increase leading to a long solution time. In [15], a McCormick relaxation was employed within a sequential bound-tightening algorithm to tackle the problem. For an unbalanced active distribution systems the convex relaxation techniques based on branch flow model cannot be applied to effectively solve the DSP under acceptable assumptions. Semidefinite programming was used in [18] to solve the DSP in an unbalanced system without considering the mutual inductance between the phases. Neglecting the voltage unbalance at system buses, semidefinite programming was applied in [13] and [19] to solve the DSP. These assumptions are not reasonable for practical systems, where voltage unbalance really matters and sometimes voltage unbalance minimization is at least considered as one of the objectives.

### B. Novelty and Contributions

- 1) to exploit the advantages of both short and long SHs using RHC technique which enables *short-term co-optimization* of the slow and fast control devices considering the system *uncertainties*.
- 2) to keep the upstream and load models up-to-date while solving the DSP.
- 3) to tailor the stochastic scheduling formulation so that the integer relaxed problems can be solved using TRA.
- 4) to compare the efficiency of the perturbed models of DCDS and their originally linear models developed using auxiliary binary variables.

### C. Paper organization

An overview of the proposed scheduling algorithm is presented in Section II. Section III presents the deterministic DSP formulation. Section IV shows how to extend this formulation to include the effects of uncertainties. Several studies are designed in Section V to test the performance of the proposed method. The conclusions are drawn and directions for future studies are outlined in Section VI.

## II. PROPOSED METHODOLOGY

### A. Uncertainty Modeling

In RHC technique, the set of scenarios of each scheduling window should be updated using the latest update on the input data. For each scheduling window, scenario generation is an iterative process along the successive periods of this window. Starting from node  $b_t$  at stage  $t$  ( $\tau \leq t \leq \tau + T - 1$ ), first a joint probability density function (PDF) is developed for the uncertain parameters at stage  $t+1$ . To form such a joint PDF, the parameters of this PDF, i.e., statistical moments such as mean values and variances, are extracted from the historical data available up until time period  $t$ . Then a single stage set of scenarios is developed using the method presented in [20] based on moment-matching technique. K-means clustering technique [20] is applied to reduce the number of single stage scenarios to keep the scenario generation tractable.

The details of developing the single stage scenarios using LP moment-matching and K-means clustering techniques were best explained in [20]. Here the process is outlined briefly. The objective in LP moment-matching technique is to find a set of scenarios for which the statistical moments are as much close as possible to the statistical moments of the joint PDF of the uncertain parameters. A large number of single stage scenarios are first generated for all uncertain parameters. Then, the probability of each scenario is determined using LP technique so that the objective of LP moment-matching technique is satisfied as much as possible. K-means clustering technique is then used to reduce the number of scenarios.

The single-stage scenario set for stage  $t+1$  that is developed from a certain node at stage  $t$  is different from the ones developed from the other nodes at stage  $t$ , since the past trend of uncertain parameters affect their future behavior. Finally, each multi-stage scenario (hereinafter called scenario) is a full trace of uncertain parameters from one of the end nodes at stage  $t=\tau+T$  back to the starting node at stage  $t=\tau$ . Considering the effects of the parent node in the single stage scenario generation process reduces the chance of unlikely variations of uncertain parameters between successive periods. This is a matter of premium importance when scheduling the DCDS, since the number of DCAs and therefore the cost of these actions depend on the rate of variation in uncertain parameters.

### B. Solution Methodology

The main focus of this paper is on providing a strategic framework for co-scheduling the fast and discrete control devices. To keep the narrative simple, some muddling aspects are neglected bearing in mind that the proposed methodology

should be able to solve the DSP with all these aspects included. It is assumed that the system is balanced. The details of applying TRA for solving unbalanced DSP were provided in [21]. The discrete variables include the tap positions, steps of CBs and additional binary variables introduced to model the tap-/step-changing costs. If the originally linear models of DCDS (subsection III-B) are applied, the respective auxiliary binary variables are also included in the list of discrete variables.

The proposed scheduling algorithm is explained step by step in the upcoming sections. An overview of this algorithm is provided here based on the comprehensive flowchart of Fig. 1. BC technique is applied to simultaneously handle the integer and continuous variables. In Fig. 1, set  $L$  (indexed by  $p$ ) is the set of all MINLP problems that should be solved during the branching process. The original problem (at the root node of BC) is given by  $\text{MINLP}^0$ .  $\Upsilon^*$  is the best integer feasible solution found so far during the branching process and  $f^* = f(\Upsilon^*)$ . In the final optimal solution point,  $f = f^{\text{opt}}$  and  $\Upsilon = \Upsilon^{\text{opt}}$ . The optimal solution of NLP problem  $p$ , optimal solution of LP problem  $p$  and a feasible solution for MINLP problem  $p$  are given by  $\Upsilon_p^{\text{NLP}}$ ,  $\Upsilon_p^{\text{LP}}$  and  $\Upsilon_p^{\text{MINLP}}$ , respectively.

In Fig. 1, the input data for the scheduling window  $\tau < t \leq \tau + T$  includes the historical data on all uncertain parameters that affect the future of the scheduling problem uncertain parameters. The input data can be divided into two categories. The first category, i.e., the historical data on the scheduling problem uncertain parameters, includes the active and reactive demands, load model parameters, utility power purchase prices, upstream system model parameters and production of each RES up until period  $\tau$ . For the upcoming periods  $t$  ( $\tau+1 \leq t \leq \tau+T$ ) these parameters are given in the scenario vectors. The second category of the input parameters includes the historical data on the external parameters. The previous values of these parameters may affect the forecast of the scheduling problem uncertain parameters for the upcoming periods. For instance, the wind speed and solar radiation in the neighbor areas during the periods up until  $\tau$  affect the forecast of wind and solar power generations within the intended system.

In Fig. 1, after generating the scenarios (see subsection II-A), a few steps are first taken to expedite the solution. The aim is to find a high quality initial solution and a tight upper bound on the value of objective function of the MINLP problem. The tighter this bound, the lower the branching burden. A simplified (linearized) problem is first solved using LP technique. A heuristic approach is then applied to change the solution to a feasible MINLP solution. In this approach, the values of discrete variables are first rounded-off to the nearest integer values. TRA is next applied to solve the resultant NLP problem and to find the values of continuous variables. Under such setup, sometimes a tighter upper bound is found for the MINLP objective function. This step is not outlined in Fig. 1 and is referred to as ‘‘applying heuristics to change  $\Upsilon_p^{\text{LP}}$  to  $\Upsilon_p^{\text{MINLP}}$ ’’.

If this step finds  $\Upsilon_p^{\text{MINLP}}$  and  $f^{\text{MINLP}} < f^*$ ,  $f^*$  is replaced with  $f^{\text{MINLP}}$ . This procedure is repeated a few times to increase the chance of obtaining a tighter upper bound. The solution

found in the previous LP is considered as the initial solution of the next one. The counter  $w_{LP}$  is used to count the LPs solved. The maximum number of LPs that are solved at this step is  $\bar{w}_{LP}$ . In the case studies,  $\bar{w}_{LP}=2$ . This  $w_{LP}$  is selected based on the experience gained by solving the scheduling problems in the studies of Section V. With higher  $\bar{w}_{LP}$ , the chance of finding a tighter bound increases. However, the higher number of LPs that should be solved may increase the solution time. Moreover, it was observed that with more than three attempts ( $\bar{w}_{LP} > 2$ ), sometimes, the solution of the LP problem starts to fluctuate. The value of  $\bar{w}_{LP}$  is set to two, so as to allow the algorithm a fair chance of attaining a tight upper bound while avoiding fluctuation and high solution times.

It is discussed in Section III how to find the model function (quadratic objective function) and perturbed objective function for TRA and simplified problem, respectively. A MILP problem is also solved using BC to further increase the chance of attaining a tight bound. This explains the steps of Fig. 2 up to point ①. The application of TRA to solve the NLPs during the branching process of BC is next explained. The respective steps are summarized in Fig. 1 between points ① and ②. These steps are better described in Fig. 2.

In Fig. 2, a globally convergent TRA is applied to solve the integer relaxed NLP problem at each node. The objective function (1) includes the operation cost, control cost and penalty terms associated with voltage deviations. The voltage deviation constraints are modeled as soft constraints using these penalty terms. The quadratic model function and perturbed constraints are built for each TRA sub-problem based on Section III. TRA first changes the inequality constraints to equality constraints [2], i.e.,  $g(\Upsilon) = 0$  in (1), using auxiliary variables. The simple bounds on optimization variables, i.e.,  $\underline{\Upsilon} \leq \Upsilon \leq \bar{\Upsilon}$  can be directly handled. In each sub-problem, TRA minimizes a model function, subjected to the perturbed constraints, within a trust region around the candidate solution of the previous sub-problem.

In Fig. 2,  $\|G\|$  gives the Euclidean norm of vector  $G$ . The integer part of real variable  $v$  is given by  $[v]$ . In each sub-problem of TRA, the problem constraints might be inconsistent with the step-size ( $\|\Delta\Psi\| \leq \alpha$ ). Byrd-Omojokun technique [2] is used to cope with the inconsistency. To this end, each sub-problem is divided into the vertical and horizontal sub-problems in Fig. 2. In the vertical sub-problem, the objective is to minimize the Euclidean norm of constraint violations within the trust region. The result of this step includes the optimal constraint violation  $\beta_i^{\min}$  for each constraint  $g_i(\Upsilon) = 0$ .

$$\underset{\Upsilon}{\text{Min}} f(\Upsilon) = \sum_{s=1}^{N_s} \pi_s \sum_{t=\tau+1}^{T+\tau} [\sigma_t OC_{t,s} + CC_{t,s} + \sum_{b=1}^{N_b} \eta_b VD_{bt,s}] \quad (1)$$

$$\text{s.t.: } g(\Upsilon) = 0, \quad \underline{\Upsilon} \leq \Upsilon \leq \bar{\Upsilon}$$

$$\Upsilon = \{v_{\tau+1}, v_{\tau+1,s}, v_{t,s} \quad \forall \tau+2 \leq t \leq T+\tau\}$$

$$\text{stopping criterion 1: } \|\nabla f(\Upsilon) + \nabla g(\Upsilon)^T \lambda\| < \epsilon_1 \quad (2)$$

$$\text{stopping criterion 2: } \|g(\Upsilon)\| < \epsilon_2 \quad (3)$$

$$\phi(\Upsilon) = f(\Upsilon) + \zeta \|g(\Upsilon)\| \quad (4)$$

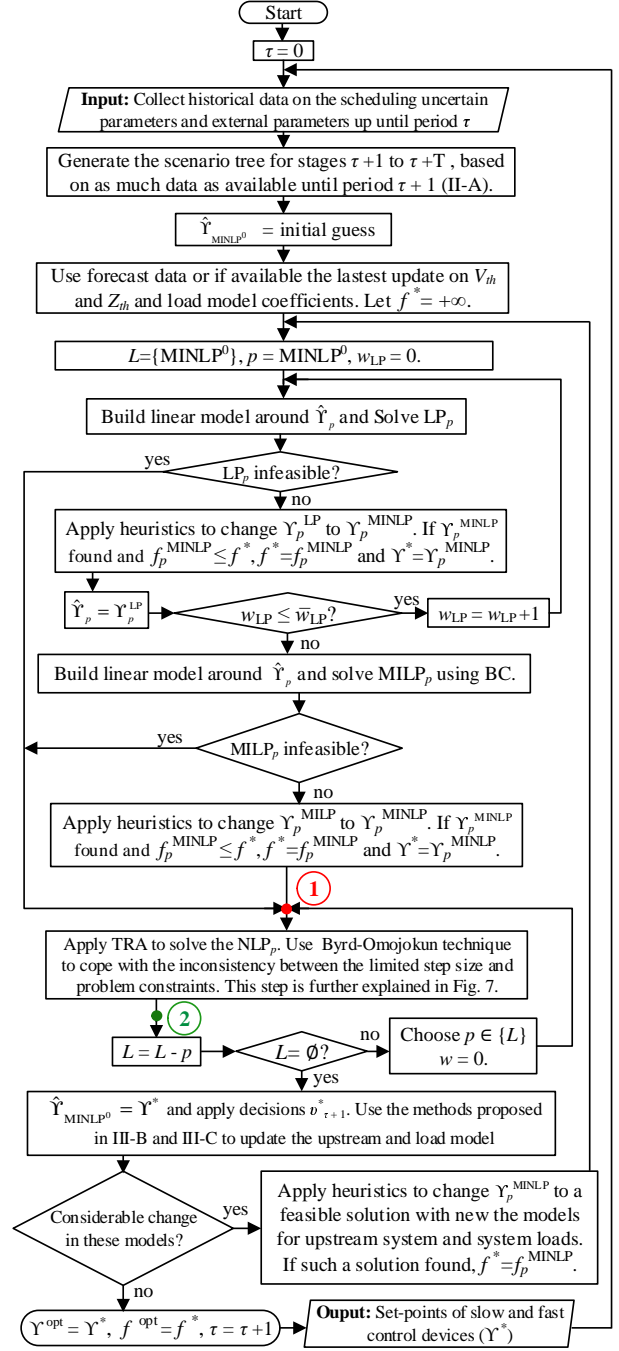


Fig. 1. Comprehensive flowchart of the proposed scheduling algorithm.

The number of TRA sub-problems solved in order to solve this NLP problem, is given by  $w$ . The maximum number of iterations is  $\bar{w}$ . The Lagrange optimality and constraints' satisfaction conditions are provided in (2) and (3), respectively. After each sub-problem, if (2) and (3) are simultaneously satisfied or  $w \geq \bar{w}$ , TRA is stopped. The Lagrange multipliers of the equality constraints of (1) are given by vector  $\lambda$ . These multipliers are not computed by TRA. A least-squares estimate is used to find  $\lambda$  based on [2]. To decide on the step size for the next TRA sub-problem, parameter  $\psi$  is used according to Fig. 2 and [2]. The merit function  $\phi(\Upsilon)$  is provided in (4).  $\zeta \geq 1$  is a penalty parameter that weights constraint satisfaction against objective minimization.

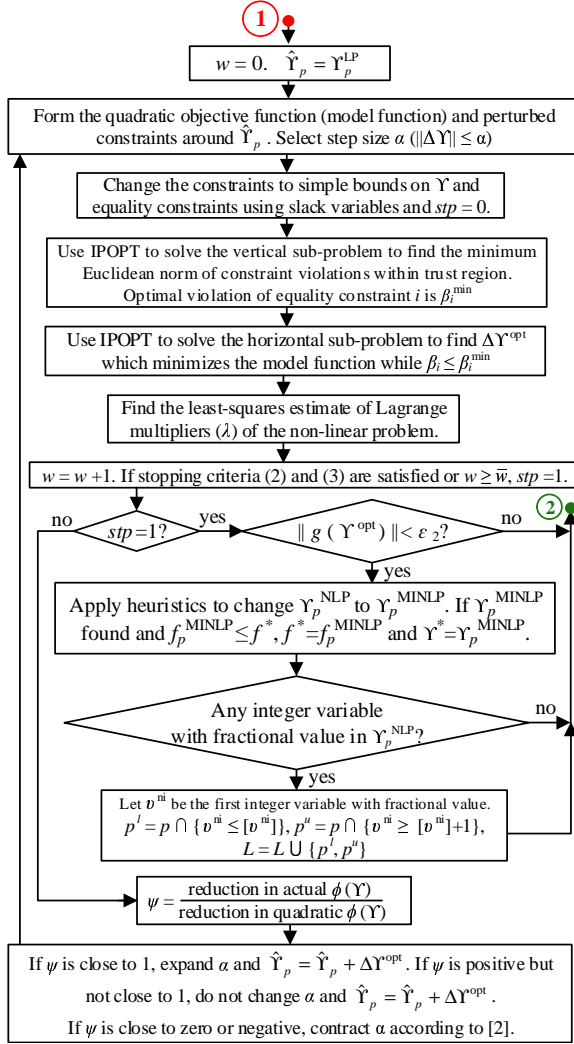


Fig. 2. Steps of TRA for solving NLP problems.

After finding the optimal solution of the MINLP problem, the parameters of upstream system and load models are updated by comparing the measured voltages and currents before and after applying  $v_{\tau+1}$  (see subsections III-B and III-C). If the changes of these models are higher than the predefined tolerances, the MINLP problem is solved again considering the previous solution as the initial guess to give BC a warm start. Only the decisions made for period  $\tau + 1$  are applied and the operator waits for further information to make the next decisions.

The expediting LPs are solved using CPLEX under GAMS. The vertical and horizontal sub-problems of TRA are solved using IPOPT under GAMS. The scheduling algorithm is implemented in MATLAB on a PC with an Intel(R) Xeon(R) E5-1650 3.6 GHz CPU and 16 GB of RAM.

### III. DETERMINISTIC SCHEDULING

The fast control devices and CBS are modeled as controllable current sources. OLTC transformer and upstream system are modeled together as a controllable current source. The network is modeled by admittance matrix. The system loads are modeled as dependent current sources. The load and upstream system models are kept updated while solving the DSP.

### A. Fast Control Devices

For fast control devices, the independent control variables include  $P_g$  and  $Q_g$ . The perturbed model is presented in (5)-(6) for a dispatchable DER.  $I$  and  $V$  are the current injected by this DER and the voltage at the connecting bus. Subscripts  $x$  and  $y$  give the real and imaginary parts, respectively. SVRS cannot exchange active power with network. It is also assumed that RESs produce as much power as the respective natural sources and their capacity constraints allow for. Thus, for SVRS and RESs the only controllable parameter is  $Q_g$  and the second term in the right hand side of (5) should be replaced with the first column of matrix  $B$  multiplied by  $\Delta Q_g$ .

$$\begin{pmatrix} \Delta I_x \\ \Delta I_y \end{pmatrix} = A_{2 \times 2} \begin{pmatrix} \Delta V_x \\ \Delta V_y \end{pmatrix} + B_{2 \times 2} \begin{pmatrix} \Delta P_g \\ \Delta Q_g \end{pmatrix} \quad (5)$$

$$A = - \begin{pmatrix} \hat{V}_x & \hat{V}_y \\ \hat{V}_y & -\hat{V}_x \end{pmatrix}^{-1} \begin{pmatrix} \hat{I}_x & \hat{I}_y \\ -\hat{I}_y & \hat{I}_x \end{pmatrix}, \quad B = \begin{pmatrix} \hat{V}_x & \hat{V}_y \\ \hat{V}_y & -\hat{V}_x \end{pmatrix}^{-1} \quad (6)$$

High quality perturbed formulations should also be developed for capacity constraints. The active power production of each RES is given in scenario vectors. The apparent power limitation of RESs is presented in (7). For each PV unit, considering the maximum power angle of  $\bar{\alpha}^{pv}$  constraints (8) should be held to avoid high harmonic distortions. As shown in (9), for a doubly-fed induction wind generator, the reactive power injection cannot be lower than a specified value. For dispatchable DERs, linear representation (10) is extracted with a desired level of accuracy using the model presented in Fig. 3. The dash-lined semicircle models the maximum apparent power that this DER can provide. This constraint is approximated by desired number of lines ( $m_n$ ,  $b_n$ ), where  $m_n$  and  $b_n$  are the slope and  $Q$ -intercept of line  $n$ . These constraints are linear and therefore, the regarding perturbed constraints are accurate. Based on Fig. 3, if the maximum apparent power constraint of DER  $e$  is approximated by  $2\bar{\pi}$  linear constraints, the maximum error of such approximation is  $(1 - \cos(\theta/4\bar{\pi}))\bar{S}^e$ . For instance, with  $\theta = 36.87^\circ$ , i.e., minimum power factor of 0.8, the maximum errors are  $0.0032\bar{S}^e$  and  $0.00051\bar{S}^e$  with  $\bar{\pi}=2$  and  $\bar{\pi}=5$ , respectively. As can be seen, this linear representation provides a quite acceptable approximation. The level of accuracy demanded by the decision maker determines  $\bar{\pi}$  based on the relationship provided for the maximum error.

$$\pm (\hat{Q}_g^{res} + \Delta Q_g^{res}) \leq \sqrt{(\bar{S}^{res})^2 - (P_g^{res})^2} \quad (7)$$

$$- \tan(\bar{\alpha}^{pv}) P_g^{pv} \leq \hat{Q}_g^{pv} + \Delta Q_g^{pv} \leq \tan(\bar{\alpha}^{pv}) P_g^{pv} \quad (8)$$

$$\underline{Q}_g^{wind} \leq \hat{Q}_g^{wind} + \Delta Q_g^{wind} \quad (9)$$

$$\begin{aligned} Q_g^{der} &\leq \tan(\theta) P_g^{der}, & Q_g^{der} &\geq -\tan(\theta) P_g^{der} \\ Q_g^{der} &\geq m_n P_g^{der} + b_n, & Q_g^{der} &\leq -m_n P_g^{der} - b_n \quad \forall n \end{aligned} \quad (10)$$

### B. Slow Control Devices

**OLTC transformer model 1:** OLTC control affects the transformer model. A perturbed model is developed here for OLTC transformers. Fig. 4 shows the  $pi$  model of an OLTC transformer connected to an upstream system with Thevenin

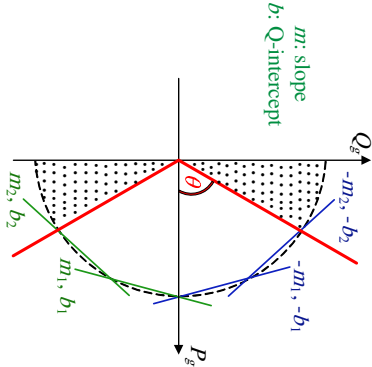


Fig. 3. Set of linear capacity constraints on dispatchable DERs with  $n=1,2$ . In the case studies, the number of linear constraints is 10, i.e.,  $\bar{n} = 5$ .

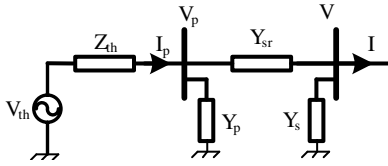


Fig. 4. Upstream network and OLTC transformer  $\pi$  models.

voltage and impedance of  $V_{th}$  and  $Z_{th}$ , respectively. A  $\pi$  model was presented in [22] for OLTC transformers. This model is extended to include the magnetizing current and core loss. The admittances of the model presented in Fig. 4 is given in (11).

It is assumed that the tap changer has been installed on the primary winding, i.e., the number of secondary turns is fixed. The transformer core is assumed to remain unsaturated. As the tap position ( $tap$ ) increases, the number of primary turns and the turn ratio ( $r$ ) increase. In the nominal tap position (given by superscript  $n$ ),  $tap^n=0$  and the turn ratio (in pu.) is 1 ( $r^n=1$ ). Tap changing operations change the per unit value of the primary series impedance ( $Z_{sr,p}$ ) proportional to the number of primary turns. The per unit value of the secondary series impedance ( $Z_{sr,s}$ ),  $X_M$  and  $R_c$  viewed from the secondary terminal do not change. It is assumed that for a well manufactured transformer  $Z_{sr,p}^n = Z_{sr,s}^n = Z_{sr}^n/2$  [22].

For OLTC transformers, the independent optimization variable is  $tap$  which is an integer variable and  $tap = (r-1)/\Delta U$ . For parallel transformers, each admittance in the  $\pi$  model is equal to the sum of regarding admittances for all transformers.

$$Y_{sr} = \frac{1}{rZ_{sr}^n}, \quad Y_p = \frac{(1-r)}{r^2Z_{sr}^n} + \frac{1}{r^2R_c^n} - \frac{j}{r^2X_M^n}, \quad Y_s = \frac{(r-1)}{rZ_{sr}^n} \quad (11)$$

$$I = C(tap)V + D(tap)V_{th} \quad (12)$$

$$\begin{pmatrix} \Delta I_x \\ \Delta I_y \end{pmatrix} = A_{2 \times 2} \begin{pmatrix} \Delta V_x \\ \Delta V_y \end{pmatrix} + B_{2 \times 1} \Delta tap, \quad A = \begin{pmatrix} C_x & -C_y \\ C_y & C_x \end{pmatrix} \quad (13)$$

$$B = \begin{pmatrix} V_x \frac{\partial C_x}{\partial tap} + V_{thx} \frac{\partial D_x}{\partial tap} - V_y \frac{\partial C_y}{\partial tap} - V_{thy} \frac{\partial D_y}{\partial tap} \\ V_y \frac{\partial C_x}{\partial tap} + V_{thy} \frac{\partial D_x}{\partial tap} + V_x \frac{\partial C_y}{\partial tap} + V_{thx} \frac{\partial D_y}{\partial tap} \end{pmatrix} \quad (14)$$

A perturbed relationship between  $I$ ,  $V$  and  $tap$  is given in (13). Matrices  $A$  and  $B$  are defined in (13) and (14), respectively. The relationship between the voltage and current at the secondary bus and the OLTC control variables ( $tap$ ) is shown in (12), where  $C$  and  $D$  can be found using Fig. 4.

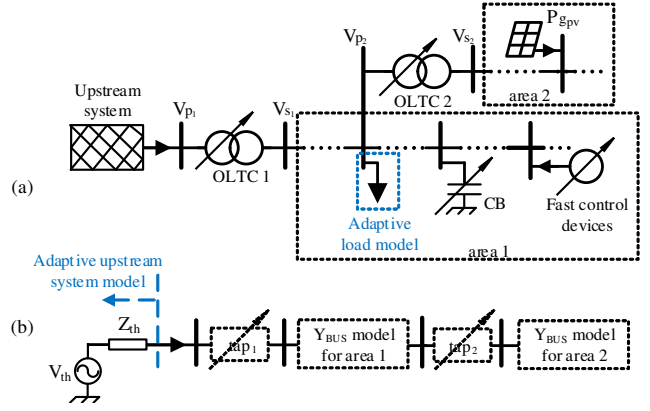


Fig. 5. a) A simple active distribution system, b) how to model OLTC transformers in active distribution systems.

In the proposed framework,  $V_{th}$  and  $Z_{th}$  are given in scenarios for  $t = \tau + 2\tau + T$ . For  $t = \tau + 1$ , it is necessary to find the accurate values of these parameters, since they affect the system model. It is important to keep  $V_{th}$  and  $Z_{th}$  up to date, while solving the DSP. By tracking the variations of measured (or estimated)  $V_p$  and  $I_p$ ,  $V_{th}$  and  $Z_{th}$  can be found, if the variations of  $V_p$  and  $I_p$  are caused dominantly by a change in the downstream network [23]. However, during the normal operation,  $V_p$  and  $I_p$  gradually change and it is not possible to understand if the source of these changes is in the downstream or upstream systems.

Based on [23],  $Z_{th}$  can be found by changing the control variables in downstream network and measuring (estimating)  $V_p$  and  $I_p$  before and after applying these changes. The changes should be significant enough to cancel the effects of measurement errors. The measurement instants should also be as close as possible to not allow the upstream system changes to affect the measured data. Here, both  $V_{th}$  and  $Z_{th}$  are found by comparing the measured values of  $V_p$  and  $I_p$ , before and after applying the changes proposed by the scheduling algorithm.

Equation (15) gives the relationship between  $V_{th}$ ,  $Z_{th}$ ,  $V_p$  and  $I_p$ . Superscripts  $\varsigma$  takes the values 0, 1, and 2. For the values before applying the changes proposed by the scheduling algorithm,  $\varsigma=0$ . For the values after applying the first and second changes,  $\varsigma$  is 1 and 2, respectively. In (15), the measured values are distinguished by a bar upon them. There are six variables, i.e.,  $\delta Z_{th}$ ,  $\delta V_p^0$ ,  $\delta V_p^1$ ,  $\delta V_p^2$ ,  $V_{th}$  and  $Z_{th}$ . With the values of 0, 1, and 2 for  $\varsigma$ , (15) gives three equations. They are rewritten in six equations separating the real and imaginary parts. Thus,  $V_{th}$  and  $Z_{th}$  are found. If the changes in  $V_{th}$  and  $Z_{th}$  are higher than a predefined level, the proposed method is applied again to solve the DSP with updated upstream model (see II-B).

$$|V_{th}|^{\angle 0} = \overline{|V_p^\varsigma|}^{\angle \delta V_p^\varsigma} + Z_{th}^{\angle \delta Z_{th}} \cdot \overline{|I_p^\varsigma|}^{\angle \delta V_p^\varsigma + \overline{\varphi}_{I_p^\varsigma, V_p^\varsigma}} \quad (15)$$

**OLTC transformer model 2:** An originally linear representation is developed here for the governing relationships of OLTC transformers using auxiliary binary variables. The results of applying this model and those obtained using the perturbed model already developed are compared in the case studies.

Both this model and the previous perturbed model can be used for the OLTC transformers like transformers 1 and 2 in

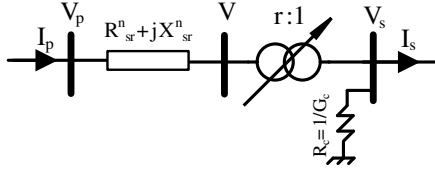


Fig. 6. OLTC transformer model 2.

Fig. 5(a) for which both primary and secondary voltages are variable, i.e., depend on control variables. For instance,  $V_{p1}$  depends on the voltage drop across  $Z_{th}$  and in turn depends on all control variables. Fig. 5(b) shows how the transformer models should be combined with the  $Y_{BUS}$  representations of the other parts of system and also the adaptive upstream model.

Fig. 6, presents OLTC transformer model used to extract the originally linear transformer equations.  $X_M$  and also the effects of tap position on series impedance are neglected. Core resistance  $R_c$  and the effects of tap-changing operations on core loss are included. This model is formulated in (16). The terms  $rV_s$  and  $rI_p$  are nonlinear which are linearized here without loss of accuracy. For brevity, the formulation is just presented for imaginary components. For real components, the same formulation can be extracted.

Variable  $r$  is a non-integer discrete variable which is rewritten in terms of dummy binary variables  $\nu_m$  in (17). The minimum turn ratio is  $\underline{r}$ . The linear counterpart of first equation in (16) is provided in (18) (imaginary component). Linear terms  $\gamma_m$  satisfies (19), where  $\sigma$  is a binary variable. For  $V_{sy} \geq 0$ ,  $\sigma=1$ .  $\overline{V_{sy}}$  is an upper bound for  $V_{sy}$ . Non-linearity of  $rI_p$  is similarly dealt with. This model is applied separately for each phase for independent per-phase OLTCs in unbalanced systems.

$$V = rV_s, \quad I_s = rI_p + G_c V_s, \quad V = V_p + (R_s + jX_s) I_p \quad (16)$$

$$r = \underbrace{1 - N_m^- \Delta U}_{\underline{r}} + \left( \sum_{m=1}^{N_m} \nu_m \right) \Delta U, \quad \nu_m \leq \nu_{m-1} \quad \forall m \quad (17)$$

$$V_y = \underline{r} V_{sy} + \Delta U \sum_{m=1}^{N_m} \gamma_m \quad (18)$$

$$\begin{aligned} (\sigma - 1) \overline{V_{sy}} &\leq V_{sy} \leq \sigma \overline{V_{sy}} \\ -\nu_m \overline{V_{sy}} &\leq \gamma_m \leq \nu_m \overline{V_{sy}} \\ \sigma \overline{V_{sy}} + V_{sy} &\leq \gamma_m \leq (1 - \sigma) \overline{V_{sy}} + V_{sy} \\ (\sigma - 1) \overline{V_{sy}} &\leq \gamma_m \leq \sigma \overline{V_{sy}} \\ V_{sy} + \overline{V_{sy}} \nu_m - \overline{V_{sy}} \sigma &\leq \gamma_m \leq V_{sy} - \overline{V_{sy}} \nu_m + \overline{V_{sy}} \sigma + \overline{V_{sy}} \end{aligned} \quad (19)$$

**Perturbed and originally linear models for CBs:** The reactive power of CBs is a function of their impedances and voltages. The perturbed model of each CB is provided in (20) and (21). An originally linear model is also developed for CBs for the sake of comparison. The non-linear model is  $I^{cb} = jy_{st} \cdot st V^{cb}$ . The term  $st V^{cb}$  is the product of integer variable  $st$  and continuous variable  $V^{cb}$ . The process of extracting the originally linear model is the same as the one used for the first equation of (16).

$$\begin{pmatrix} \Delta I_x \\ \Delta I_y \end{pmatrix} = A_{2 \times 2}^{cb} \begin{pmatrix} \Delta V_x \\ \Delta V_y \end{pmatrix} + B_{2 \times 1}^{cb} \Delta st \quad (20)$$

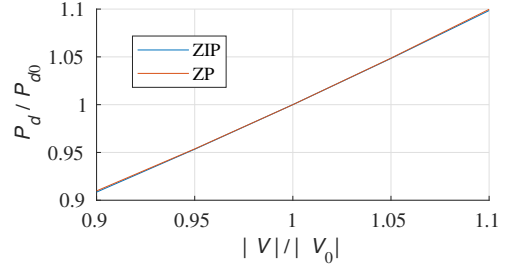


Fig. 7. Comparison between ZIP and ZP model based on the data collected from a real-life distribution system.

$$A^{cb} = \begin{pmatrix} 0 & st \cdot y^{st} \\ -st \cdot y^{st} & 0 \end{pmatrix}, \quad B^{cb} = \begin{pmatrix} y^{st} V_y \\ -y^{st} V_x \end{pmatrix} \quad (21)$$

### C. Adaptive Load Model

Power demands depend on the voltage levels at load points. Load model accuracy affects the solution optimality. With an inaccurate model, the expected energy saving is not realized. ZIP model (22) which decomposes the system loads into constant impedance, constant current and constant power components [24] is applied here. In (22),  $a_p + b_p + c_p = a_q + b_q + c_q = 1$ . To keep the simplicity of presentation, this ZIP load model is replaced by a ZP model. Replacing  $|V|/V_0$  by  $0.5(1+|V|^2/V_0^2)$  in (22), ZP load model is provided in (23). Comparing (23) with (22),  $a'_p = a_p + b_p/2$ ,  $c'_p = c_p + b_p/2$  and  $a'_p + c'_p = a'_q + c'_q = 1$ . Within the typical range of bus voltages in the steady state studies, the accuracies of ZIP and ZP models are quite close and (23) gives a quite acceptable approximation of (22). For instance, with  $|V|/V_0=0.9$  which is a voltage drop condition that might never happen in the steady state operation of distribution systems,  $0.5(1+|V|^2/V_0^2)=0.905$ . For the voltages closer to unity, this approximation is even more accurate.

Moreover, only a small share of distribution loads is constant current. Here the accuracies of ZP and ZIP models are compared in practice based on the minute-by-minute data collected from the load points of a real-life distribution system in Dublin, Ireland [25]. Coefficients  $a$ ,  $b$ , and  $c$  are estimated for every minute of a sample day at all load points, using the high-resolution measured data records. Fig. 7 presents the average of  $P_d^t/P_{d0}^t$  found based on both ZIP and ZP models for  $t=1:1440$  minutes. Considering the same chance for all possible values of  $|V|/V_0$  in the range of  $[0.9 \ 1.1]$ , the standard deviation of normalized active powers calculated using ZP model compared with the ZIP counterparts is 0.057%. The maximum deviation of active powers calculated with ZP model with respect to the ZIP counterparts is 0.17%. With the minute-by-minute measured voltages taken into account, these standard and maximum deviations are 0.021 and 0.028%, respectively. However, if the level of accuracy that ZP model or even ZIP model provides is not sufficient, more accurate voltage-dependent load models can be applied. The proposed method can easily accommodate any load model with desired level of complexity and accuracy.

The voltage-dependent behavior is not fixed and the model should be kept up to date. Coefficients  $a'_p$  and  $c'_p$  and  $a'_q$  and  $c'_q$  are not independent, i.e.,  $a'_p + c'_p = a'_q + c'_q = 1$ .

Therefore, in order to update this model for  $t=\tau+1$ , four coefficients should be determined, i.e.,  $a'_p$ ,  $P_{d_0}$ ,  $a'_q$ , and  $Q_{d_0}$ . Two sets of measurements for  $P_d$ ,  $Q_d$  and  $V$  are required. The first/second set of parameters is measured before/after applying the changes proposed by the scheduling framework. The following algorithm updates the model for  $t=\tau+1$ .

- 1) Consider the values forecasted for or the last update of  $a'_p$  and  $a'_q$ .
- 2) Measure/estimate  $|V|$ ,  $P_d$  and  $Q_d$  and calculate  $P_{d_0}$  and  $Q_{d_0}$  using (23).
- 3) Solve the DSP with this load model for  $t=\tau+1$ , and the load model given in the scenarios for  $t = \tau + 2:\tau + T$ .
- 4) Apply the set-points proposed.
- 5) Measure/estimate  $|V|$ ,  $P_d$  and  $Q_d$ .
- 6) Two sets of measurements are now available from steps 2 and 5. Use the first equation of (23) with these two sets of measurements to update  $a'_p$  and  $P_{d_0}$ . Use the second equation of (23) to update  $a'_q$  and  $Q_{d_0}$ .
- 7) If the change in the updated values is not negligible, solve the DSP again using the updated load model coefficients.

The values of  $|V|$ ,  $P_d$  and  $Q_d$  are not measured at all buses. In case that there are enough measurements, state estimation techniques, such as those reviewed in [26], can be applied to approximate these values for the buses at which these parameters are not measured. If this is not the case, the load model coefficients for period  $\tau + 1$  should also be included in the scenario vectors in the same way as periods  $\tau+1:\tau+T$ . The method that is presented here for updating the load model for period  $\tau + 1$  can still be used to reduce the degree of uncertainties on these parameters. Using the limited number of measurements before and after applying the optimal changes, historical data, system physical equations and equations (23), state estimation techniques can approximate the mean values and standard deviations of the load model coefficients in period  $\tau + 1$ . These statistical moments can be used to extract the scenarios on these coefficients along with the other uncertain parameters using the method presented in subsection II-A.

This paper deals with the DSP and steady state voltage control problem. In the real time operation of distribution systems, some other effects, e.g., dynamic voltage stability and harmonic distortion issues, may need to be taken into account. To deal with such issues, dynamic and nonlinear load models should be applied, respectively. Dynamic and non-linear control techniques and load models cannot be used for steady state voltage control. In the DSP and steady state voltage control problem, the voltage-dependent behavior of loads needs to be taken into account. ZIP model is applied to formulate the nonlinear relationship between the load and voltage levels with an acceptable accuracy. The loads can be of any types. The ZIP coefficients at each load point depend on many factors and change from time to time. For instance, the ZIP coefficients of a motor load depend on motor type, size, load and speed. For every load point, the coefficients are estimated for period  $\tau + 1$  and are included in the scenarios for  $\tau + 2:\tau + T$ .

The equation of apparent power demand at each network bus is given in (24). The negative sign indicates that  $P_d$  and

$Q_d$  are consumed. Combining the perturbed counterparts of (23) and (24), the perturbed load model is given in (25).

$$\frac{P_d}{P_{d_0}} = a_p \frac{|V|^2}{V_0^2} + b_p \frac{|V|}{V_0} + c_p, \quad \frac{Q_d}{Q_{d_0}} = a_q \frac{|V|^2}{V_0^2} + b_q \frac{|V|}{V_0} + c_q \quad (22)$$

$$\frac{P_d}{P_{d_0}} = a'_p \frac{|V|^2}{V_0^2} + c'_p, \quad \frac{Q_d}{Q_{d_0}} = a'_q \frac{|V|^2}{V_0^2} + c'_q \quad (23)$$

$$P_d + jQ_d = -VI^* \quad (24)$$

$$\begin{pmatrix} \Delta I_x \\ \Delta I_y \end{pmatrix} = \begin{pmatrix} \hat{V}_x & \hat{V}_y \\ \hat{V}_y & -\hat{V}_x \end{pmatrix}^{-1} \begin{pmatrix} \frac{2a'_p P_{d_0} \hat{V}_x}{V_0^2} - \hat{I}_x & \frac{2a'_p P_{d_0} \hat{V}_y}{V_0^2} - \hat{I}_y \\ \frac{2a'_q Q_{d_0} \hat{V}_x}{V_0^2} + \hat{I}_y & \frac{2a'_q Q_{d_0} \hat{V}_y}{V_0^2} - \hat{I}_x \end{pmatrix} \begin{pmatrix} \Delta V_x \\ \Delta V_y \end{pmatrix} \quad (25)$$

#### D. Objective Function and Perturbed Constraints

Here, the objective is to minimize the system cost for the deterministic single-period DSP and is given in (26). It is shown in Section IV how to extend this formulation to achieve the formulation of stochastic DSP. The objective function includes the change in the operation cost ( $\Delta OC_t$ ) and control cost ( $CC_t$ ) due to changing the control variables from  $\hat{v}_t$  to  $v_t$ .  $\Delta OC_t$  and  $CC_t$  are presented in (27) and (28), respectively. The voltage constraints are modeled as soft constraints, i.e., the voltage deviations are penalized in the objective function.

Binary variables  $u_{k_{TC}}$  and  $u_{k_{CB}}$  should satisfy (29) and (30). In (29),  $\Delta tap_{k_{TC}}^{max}$  is the maximum possible tap change. If such parameter does not exist for the transformer,  $\Delta tap_{k_{TC}}^{max} = \overline{tap_{k_{TC}}} - \underline{tap_{k_{TC}}}$ . The perturbed voltage constraints at bus  $b$  are given in (31). The current constraint of line  $l$  is given in (32). Neglecting the small term  $(\Delta V_{1x} - \Delta V_{2x})(\Delta V_{1y} - \Delta V_{2y})$ , a perturbed formulation for the maximum current constraint is provided in (33). For simplicity, the index  $t$  has been removed from (31) and (33). The sending and receiving buses are given by subscripts 1 and 2, respectively. As shown in (34), the tap positions and CB steps should be set within their limits.

It is imperative to distinguish between  $\hat{v}_t$  and  $v_{t-1}$ . For instance, in (29),  $\hat{tap}_{k_{TC},t}$  is the tap position of transformer  $k_{TC}$  in period  $t$  that is found in the previous sub-problem of TRA or is included in the initial guess.  $tap_{k_{TC},t-1}$  is the tap position in the previous period. The model function and perturbed constraints are built around  $\hat{v}_t$ .

$$\underbrace{Min}_{v_t} \{F_{D,t}\} = \sigma_t \Delta OC_t + CC_t + \sum_{b=1}^{N_b} \eta_b [\underline{\vartheta}_b + \overline{\vartheta}_b] \quad (26)$$

$$\Delta OC_t = \rho_{A_t} \Delta P_{p_t} + \rho_{R_t} \Delta Q_{p_t} + \sum_{e \in DER} \rho_e \Delta P_{g_e,t} \quad (27)$$

$$CC_t = \sum_{k_{TC} \in OLTC} u_{k_{TC},t} D_{k_{TC}} + \sum_{k_{CB} \in CB} u_{k_{CB},t} D_{k_{CB}} \quad (28)$$

$$\Delta tap_{k_{TC},t} + \hat{tap}_{k_{TC},t} - tap_{k_{TC},t-1} \leq u_{k_{TC},t} \Delta tap_{k_{TC}}^{max} \\ - \Delta tap_{k_{TC},t} - \hat{tap}_{k_{TC},t} + tap_{k_{TC},t-1} \leq u_{k_{TC},t} \Delta tap_{k_{TC}}^{max} \quad (29)$$

$$\Delta st_{k_{CB},t} + \hat{st}_{k_{CB},t} - st_{k_{CB},t-1} \leq u_{k_{CB},t} \Delta st_{k_{CB}}^{max} \\ - \Delta st_{k_{CB},t} - \hat{st}_{k_{CB},t} + st_{k_{CB},t-1} \leq u_{k_{CB},t} \Delta st_{k_{CB}}^{max} \quad (30)$$

$$\underline{V}_b^2 - |\hat{V}_b|^2 - \underline{\vartheta}_b \leq 2\hat{V}_{b_x} \Delta V_{b_x} + 2\hat{V}_{b_y} \Delta V_{b_y} \leq \overline{V}_b^2 - |\hat{V}_b|^2 + \overline{\vartheta}_b \quad (31)$$

$$|V_1 - V_2|^2 \leq (R_l^2 + X_l^2) \overline{I}_l^2 \quad (32)$$

$$(\hat{V}_{1x}-\hat{V}_{2x})\Delta V_{1x}+(\hat{V}_{1x}-\hat{V}_{2x})\Delta V_{2x} \\ +(\hat{V}_{1y}-\hat{V}_{2y})\Delta V_{1y}+(\hat{V}_{1y}-\hat{V}_{2y})\Delta V_{2y}\leq(R_l^2+X_l^2)\frac{\overline{I}_l^2-|\hat{I}_l|^2}{2} \quad (33)$$

$$\overline{tap}_{k_{TC}}\leq\hat{tap}_{k_{TC},t}+\Delta tap_{k_{TC},t}\leq\overline{tap}_{k_{TC}} \\ \underline{st}_{k_{CB}}\leq\hat{st}_{k_{CB},t}+\Delta st_{k_{CB},t}\leq\overline{st}_{k_{CB}} \quad (34)$$

The perturbed voltages and currents in this formulation are rewritten in terms of the optimization variables by combining the models extracted for the controllable devices and system loads with the network model provided in (35). The non-perturbed notations are constant. The perturbed currents in (35) are replaced by the perturbed control variables and voltages using the perturbed equations presented for the controllable devices and loads. The resultant equations would be (36) and (37).  $\Upsilon$  and  $N_v$  are the vector and number of control variables, respectively. Matrices  $\mathbf{A}$  and  $\mathbf{B}$  are found using matrices  $\mathbf{A}$  and  $\mathbf{B}$  developed for the controllable devices and loads.

As discussed in subsection II-B, to apply TRA, all inequality constraints should be converted to equality constraints using auxiliary variables. Simple bounds on the optimization variables can also be handled. For instance, (31) is converted to (38) using positive auxiliary variables  $\overline{\epsilon}_b$  and  $\underline{\epsilon}_b$ .

$$\begin{pmatrix} \Delta I_x \\ \Delta I_y \end{pmatrix}_{2N_b \times 1} = \underbrace{\begin{pmatrix} Y_{Busx} & -Y_{Busy} \\ Y_{Busy} & Y_{Busx} \end{pmatrix}}_{\mathbf{Y}} \cdot \begin{pmatrix} \Delta V_x \\ \Delta V_y \end{pmatrix}_{2N_b \times 1} \quad (35)$$

$$\mathbf{A} \begin{pmatrix} \Delta V_x \\ \Delta V_y \end{pmatrix} + [\mathbf{B}]_{2N_b \times 2N_v} [\Upsilon]_{2N_v \times 1} = \mathbf{Y} \begin{pmatrix} \Delta V_x \\ \Delta V_y \end{pmatrix} \quad (36)$$

$$\begin{pmatrix} \Delta V_x \\ \Delta V_y \end{pmatrix} = (\mathbf{Y} - \mathbf{A})^{-1} \mathbf{B} \cdot \Upsilon \quad (37)$$

$$2V_{bx}\Delta V_{bx}+2V_{by}\Delta V_{by}-\overline{v}_b+\overline{\epsilon}_b=\overline{V}_b^2-|V_b|^2, \quad \overline{\epsilon}_b \geq 0 \\ 2V_{bx}\Delta V_{bx}+2V_{by}\Delta V_{by}+\underline{v}_b-\underline{\epsilon}_b=\underline{V}_b^2-|V_b|^2, \quad \underline{\epsilon}_b \geq 0 \quad (38)$$

In TRA sub-problems, the model function is a quadratic function of perturbed optimization variables. In (27),  $\Delta P_{pt}$  and  $\Delta Q_{pt}$  are non-linear in terms of optimization variables.  $\Delta P_{pt}$  and  $\Delta Q_{pt}$  can be replaced by  $\Delta V_{pt}$  and  $\Delta I_{pt}$  using  $P_{pt}+jQ_{pt}=V_{pt}I_{pt}^*$ .  $V_{pt}$  is the voltage at and  $I_{pt}$  is the current injected to the primary side of transformer. Using the model developed for OLTC transformers,  $\Delta V_{pt}$  and  $\Delta I_{pt}$  are rewritten in terms of  $\Delta V_{st}$  and  $\Delta I_{st}$  and  $\Delta tap_t$ .  $\Delta V_{st}$  and  $\Delta I_{st}$  are rewritten in terms of the perturbed control variables using (37).

#### IV. STOCHASTIC SCHEDULING

The objective function of the proposed stochastic scheduling algorithm is given in (39). To make a compromise between the solution accuracy and computational burden,  $\sigma_t$  is increased as  $t$  increases. In a day-ahead formulation for the DSP, in every time period, the OLTC(s') tap position(s) are the same for all scenarios. However, in the proposed RHC-based method, only the tap positions found for the first period ( $\tau+1$ ) are the same for all scenario. The reason is that only the decisions made for this period are really applied. Therefore, except for  $tap_{\tau+1}$  the tap positions for other periods take subscript  $s$ .

More details were provided in Section II. All the constraints introduced for the deterministic single period DSP should also

be included. Constraint (29) is rewritten as (40)-(41), where the point  $\hat{v}$  is the initial point to build the perturbed model (or the solution of the previous TRA sub-problem) around it. Subscript  $k_{TC}$  is removed for brevity. Constraint (30) is rewritten similarly. Only the decisions taken for period  $\tau+1$  are implemented and the proposed algorithm is applied again to extract the optimal schedule of the next period. The number of tap changing operations is limited using (42). For CBs, the same constraints are considered.

$$\underset{\Upsilon}{Min} \{F_{S\tau}\} = \sum_{s=1}^{N_s} \pi_s \sum_{t=\tau+1}^{\tau+T} (\sigma_t \Delta OC_{t,s} + CC_{t,s}) \\ + \sum_{s=1}^{N_s} \pi_s \sum_{b=1}^{N_b} \eta_b \left[ \overline{v}_{bt,s} + \underline{v}_{bt,s} \right] \quad (39)$$

$$\Upsilon = \{v_{\tau+1}, v_{\tau+1,s}, v_{t,s} \quad \forall \tau+2 \leq t \leq T+\tau\}$$

$$\forall s, t \geq \tau+2 \\ \Delta tap_{s,t} - \Delta tap_{s,t-1} + \hat{tap}_{s,t} - \hat{tap}_{s,t-1} \leq u_{s,t} \Delta tap^{max} \\ \Delta tap_{s,t-1} - \Delta tap_{s,t} - \hat{tap}_{s,t} + \hat{tap}_{s,t-1} \leq u_{s,t} \Delta tap^{max} \quad (40)$$

$$\Delta tap_{\tau+1} + \hat{tap}_{\tau+1} - tap_{\tau} \leq u_{\tau+1} \Delta tap^{max} \\ -\Delta tap_{\tau+1} - \hat{tap}_{\tau+1} + tap_{\tau} \leq u_{\tau+1} \Delta tap^{max} \quad (41)$$

$$u_{k_{TC},\tau+1} + \sum_{t=\tau+2}^{T+\tau} u_{k_{TC},s,t} \leq \overline{N}_{TC\tau} \quad \forall s \quad (42)$$

#### V. CASE STUDIES

The proposed algorithm is tested on IEEE 33-bus test system. Table I presents the data of two parallel OLTC transformers which connect this system to the upstream network and a DER, a PV unit, a CB and an SVR which are added to this system. The average hourly load levels and energy prices are presented in Fig. 8(a) and  $\rho_R=0.2\rho_A$ . The average coefficients of ZIP model is found in [24]. The PV unit produces active power from 7 AM to 7 PM. The maximum producible power ( $\overline{S}_{PV}$ ) happens at 1 PM. From 6 AM to 1 PM and from 1 PM to 8 PM,  $P_g^{PV}$  changes linearly from zero to  $\overline{S}_{PV}$  and from  $\overline{S}_{PV}$  to 0, respectively. Fig. 10 (a) shows the average upstream Thevenin voltage levels.  $\overline{V}=1.05$ ,  $\underline{V}=0.95$  and  $\sigma=1$  h.

So far, the average values ( $\mu$ ) of all uncertain parameters have been presented. A forecast error of  $e_{t,\xi}$  is assigned to uncertain parameter  $\xi$  at period  $t$ . For the first period ( $t = \tau+1$ ),  $e_{\tau+1,\xi} = 0.02\mu_{\tau+1,\xi}$ . This forecast error increases linearly for the upcoming periods with the rate of  $0.1e_{\tau+1,\xi}$  per period. The uncertainty of the parameters is modeled using a joint normal PDF with the average values of  $\mu_t$  and standard deviations of  $e_t$ . The correlation between the load levels at each two buses at a certain period is considered to be 80%. The correlation between the load levels at a certain bus and  $V_{th}$ ,  $Z_{th}$ , active power prices and reactive power prices at successive time periods are considered to be 70, 90, 80, 90 and 90%, respectively. Other correlations are not taken into account.

The proposed algorithm is applied from 1 AM with an infeasible starting point ( $tap_1=tap_2=0$ ,  $st=3$ ,  $P_g^{DER}=Q_g^{DER}=Q_g^{PV}=0$  and  $Q_g^{SVR}=300$  kVAR). In all studies, the proposed framework is applied 24 times. In the

TABLE I  
CONTROLLABLE DEVICES AND DSP PARAMETERS

	Bus	Characteristics
DER	14	$S=500$ kVA, $P_g=500$ kW, $Q_g=50$ kVAR, $\rho=60$ €/MWh
PV	14	$S=250$ kVA, $P_g=250$ kW, $\alpha^{pv}=35^\circ$
SVR	30	$Q_g=500$ kVAR
CB	33	$Q_g=500$ kVAR, $st=5$

$Z_{sr}^n=Z_{th}^n=0.01+0.05j$ ,  $tap=3$ ,  $\underline{tap}=-3$ ,  $\Delta U=1\%$ ,  $R_V^n=100$  and  $X_M^n=95$  pu.  
 $T=20$  h,  $\sigma=1$  h,  $D_{OLTC}=\epsilon=20$ ,  $D_{CB}=\epsilon=10$ ,  $\bar{V}=1.05$ ,  $\underline{V}=0.95$

TABLE II  
CASE STUDIES

Case	Load Model	$D_{OLTC}$ (€)	$D_{CB}$ (€)	$T$ (h)	OC (€)	DCC (€)	Cost (€)	Loss (MWh)
1	ZIP	20	10	20	4931.4	50.0	4981.4	2.11
2	ZIP	20	10	1	4973.3	50.0	5023.3	2.36
3	ZIP	-	-	20	4883.9	190.0	5073.9	2.12
4	ZIP	40	20	20	4931.4	100	5031.4	2.11
5	P	20	10	20	5136.3	30.0	5166.3	2.96
0*	ZIP	20	10	20	5032.1	50.0	5082.1	2.22

\* Case 0 with Inaccurate Upstream Model

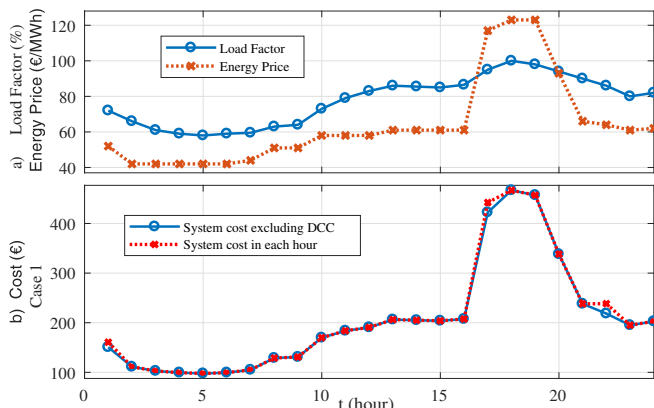


Fig. 8. a) Load factors and energy prices, b) system costs in Case 1.

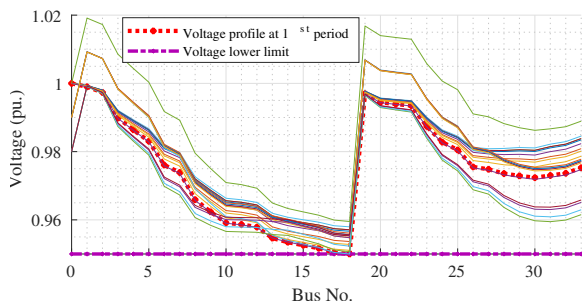


Fig. 9. Voltage profiles for  $t=1-20$  in the first scheduling window.

first study the SH ( $T$ ) is 20 hours. It can be assumed that a 20-hour scheduling window is being moved hour by hour to solve the DSP, considering the system future. For some hours, a certain length of this window happens in the next day with all parameters same as those specified for the current day.

Six different studies, i.e., cases 1-5 and case 0, are conducted (see Table II). In cases 1-5, the results of applying the proposed algorithm are provided in Figs. 8-12. Fig. 8 presents the total costs and discrete control costs (DCCs) in Case 1 along with the average energy prices and load factors. Fig. 9 gives the voltage profiles in case 1 for hours  $t=1:20$ , i.e., the first scheduling window, for the most probable scenario. Each voltage profile corresponds to one of the periods  $t=1:20$ . The main purpose of this figure is to show the voltages never

violate the limits and to identify the bus with the minimum voltage level. Fig. 10 shows the DCAs to analyze the effects of changing the parameters of the proposed algorithm. In this figure, the variations of the average Thevenin voltages of the upstream system are also presented. The production levels of the DER are presented in Fig. 11. The results provided in Figs. 11 and 10 show the interconnections between the discrete and continuous control actions in the simultaneous scheduling of fast and slow control devices. Fig. 12 compares the total costs and energy losses. These total costs and energy losses are also presented in Table II along with the operation costs (OCs) and DCCs.

**In Case 1**, at the first period, the framework proposes the cheapest actions. The CB step is increased by two steps in Fig. 10 (c) and  $P_g^{der}$  is raised by 80 kW in Fig. 11. These control actions solve the under-voltage issues for the initial time periods. Meanwhile, the voltage profiles are kept as low as possible, of course, without violating the lower bound voltage limit. This reduces the power demand considering the voltage-dependent nature of the loads. Fig. 9 presents the voltage profiles for all periods ( $t=1:20$ ) in the first scheduling window for the most probable scenario. The voltage at bus 18 hits the minimum level in some initial periods ( $V_{t=1,b=18}=0.95$  pu).

According to Fig. 11, from period 9 to 13, the load increases and the production of DER is raised to avoid under-voltages. Especially,  $P_g^{der}$  jumps from 191 to 423 kW to avoid under-voltage issues due to the upstream voltage drop shown in Fig. 10 (a). From period 13 to 15,  $P_g^{der}$  is slightly decreased since the load level slightly decreases.  $P_g^{der}$  increases again in period 16, as does the load level. At period 17, the upstream voltage drops for the second time and the load level widely increases. It is not now possible to hold the voltages within the limits without tap-changing operations. Fig. 10 (b) shows the tap-changing operations for all periods. Instead of 1 step, the tap position is reduced by 2 steps to avoid the additional cost of another tap-changing operation for higher load levels. Finally, the framework proposes to increase the tap position to reduce the voltage level after the upstream voltage is restored to 1 pu. This reduces the operation cost, since the load levels decrease due to load-to-voltage dependence. This OC reduction for the remaining periods of the current day and early hours of the next day is worth spending the tap-changing cost. With a short scheduling window ( $T$ ), the scheduling algorithm has no vision of the upcoming periods and avoids spending this tap-changing cost. This leads to higher operation cost. In case 2, the effects of such a short scheduling window are further analyzed.

**In Case 2**, the SH is considered to be 1 hour, signifying no vision of the system future. The tap position is reduced at period 17 to cope with voltage reduction at upstream system (see Fig. 10(b)). If the scheduling algorithm was able to see only one more period ahead, the tap position would be reduced by 2 steps. Since in the next period, the load level increases and the tap position should be lowered again. The CB step is increased one time to avoid under voltage during the heavy-load periods. The daily OC is also higher in this case (Table II) since the tap changing operations are not justified just for

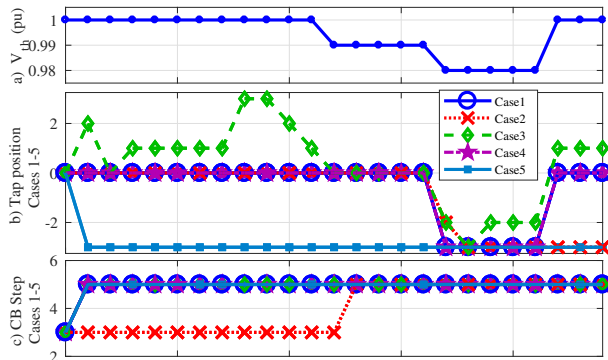


Fig. 10. a) Upstream system voltages, b) OLTC tap positions, c) CB steps.

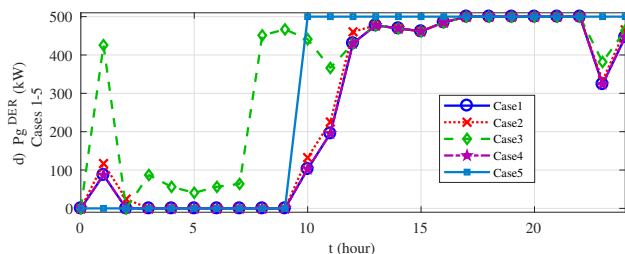


Fig. 11. Power productions of the dispatchable DER.

a single period while these control actions were able to reduce the cost for  $t=21:24$  as explained in case 1.

**Case 3** is designed to show the necessity of considering the DCC in the objective function. The DCC is just excluded from the objective function. For calculating the total cost in Table II, the DCC is included. As can be seen in Fig. 10 (b), the tap position is freely changed according to the load pattern, upstream system voltage and  $\rho_A$ . The results shows that if the DCC is not taken into account, a lower OC is achieved. However, the higher DCC increases the total cost.

The interactions between the tap-changing operations and the power output of the DER in this study are also interesting. In order to better understand this interconnections, the load levels and  $\rho_A$  (presented in Fig. 8) should also be taken into account. In period 1,  $\rho_A$  is relatively high. The scheduling algorithm takes the opportunity to reduce the system cost, by reducing the voltage at substation level. To avoid under-voltages at bus 18,  $P_g^{der}$  is increased.  $\rho_A$  is even lower than  $\rho_{der}=60$  (€/MWh). However, the load reduction due to increasing the tap position is worth spending more money on supplying a part of the system demand by the DER in this period. For period 2, the average  $\rho_A$  decreases and supplying a part of the system demand by the DER is not justified. For periods 3-7 the load level is lower and therefore, with a low  $P_g^{der}$  the under-voltage at bus 18 is avoided. Increasing  $P_g^{der}$  increases the OC, but the load reduction due to the tap increase justifies the solutions shown in Figs. 10 and 11 for these periods. With higher  $\rho_A$  and lower  $P_d$  in period 8, the tap position is increased by two steps and  $P_g^{der}$  is increased again to avoid under-voltages.

**Case 4:** In case 1, relatively high  $D_{OLTC}$  and  $D_{CB}$  were deliberately selected (considering 3 tap changing operations per day,  $D_{OLTC}=\text{€}20$ , is equivalent to maintenance cost of

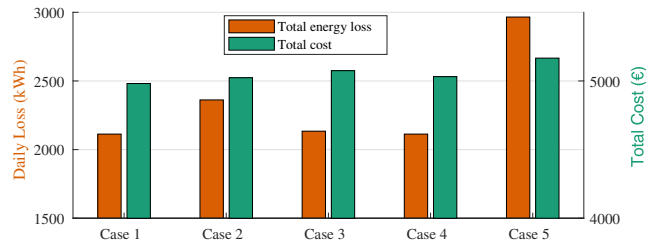


Fig. 12. Energy loss and total cost in Cases 1-5.

660 (€/1000/year) for the OLTC transformers). To show that with the higher prices for DCAs, the proposed algorithm is still able to reduce the cost, the simulations are repeated with  $D_{OLTC}=\text{€}40$  and  $D_{CB}=\text{€}20$ , and the exact same results were found. The only difference between cases 1 and 4 is on their DCC (Table II) due to the different discrete control prices.

**In Case 5**, the load-to-voltage dependence is neglected. This means  $a'$  is set to 0 in the scheduling algorithm. However, the OC is calculated in Table II with the real values of the load model parameters. With  $a'=0$ , the load levels are assumed to be independent of the voltage levels. Therefore, the algorithm increases the voltage levels to reduce the load current and network losses. The tap position and CB step are set to the lowest and highest values, respectively. Though this leads to the lower DCC, the system OC and total cost are higher according to Table II. As shown in Fig. 12, even the loss reduction is not realized in reality by this inaccurate load model.

#### A. Effects of Inaccurate Upstream System Models

This subsection discusses what happens in case of applying an inaccurate upstream model. One option is to consider the voltage of the primary side as the Thevenin voltage neglecting the Thevenin impedance. This study is referred to as Case 0. To extract the results for Case 0, at the start of each period,  $V_p$  is calculated considering a  $Z_{th}$  equal to the one considered for Cases 1-5 and the Thevenin voltage shown in Fig. 10(b). This step is designed to find the values of  $V_p$ . In reality these values are found through the measurements. Then the proposed algorithm is applied assuming  $Z_{th}=0$  and  $V_{th}=V_p$ . When the solution is found, the line currents, bus voltages, power losses and system cost are calculated assuming a  $Z_{th}$  equal to the one considered for Cases 1-5. This approach is applied for all 24 hours of the current day with  $T=20$  hours. Table II shows that the system cost would be about 2% higher comparing to Case 1. To elaborate, it should be noted that with  $Z_{th}=0$ ,  $V_p$  would remain fixed as the control parameters are changed in downstream network. However, in reality, by applying the changes, the primary current varies, and sometimes the actual value of  $V_p$  is lower/higher than the assumed fixed value and therefore, due to the voltage dependent characteristics of the system loads, the demand would be lower/higher. The control plans at different periods are also different from Case 1.

This simplified upstream model also leads to voltage constraints violations. According to Fig. 9, bus 18 has the lowest voltage level. Fig. 13 shows the 24-hour voltage profile at this bus for all cases in the most probable scenario. In Cases

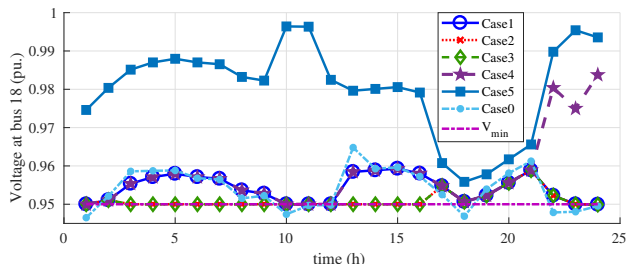


Fig. 13. Voltage level at bus 18 for  $\tau = 0$  and periods 1-24.

1-5, there is no under-voltage issue. The under-voltage issue observed in Case 0 shows that without an accurate upstream model, the solutions can be infeasible. The upstream models should also be kept up-to-date. Another important observation is that based on Fig. 13, for Case 0 and Cases 1-4, the proposed scheduling framework has tried to keep the voltage level as low as possible to reduce the system demand and system cost. In Case 5, the voltage levels at this bus are higher due to neglecting the voltage dependent nature of the system loads.

### B. Effects of Load Characteristics

Fig. 14 shows the daily costs, i.e., the sum of system costs for the first hour of all 24 scheduling windows for different values of the constant impedance share ( $a'$ ) of system load.  $a' = 0$  indicates a fully constant power load. Comparison of these costs for  $T=1, 10, 20$  h, gives an insight into the importance of applying the proposed method based on RHC. The results of previous sections show that the voltage-dependent nature of loads can be deemed as an opportunity to reduce the operation cost. With  $T=1$ , in some cases, the system costs increase as  $a'$  increases. The reason lies in the fact that with  $T=1$ , the scheduling framework is unable to take the future operation conditions into account and makes greedy decisions for the early stages which condemn moving towards the optimal operation conditions in the upcoming periods since the required changes are not justified due to their high cost.

As  $a'$  increases, the cost reduction is steeper for some values. These steeper cost reductions happen due to cost-reducing DCAs. To elaborate, for some values of  $a'$ , cost-reducing DCAs might be available, but it might not be possible to apply them due to constraints violations. Increasing the tap position (which reduces the voltage levels) can be considered as one of these DCAs. For the higher values of  $a'$ , after applying these cost-reducing DCAs, voltage levels are lower. These lower voltages reduce the active and reactive power demands due to the voltage-dependent nature of loads. Since  $a'$  is relatively high, these demand reductions are considerable. These demand reductions increases the voltage levels so that at a lower demand level, the bus voltages are acceptable according to the standard.

### C. Performance of the Proposed Solution Methodology

The solution times of each scheduling windows ( $T=20$  h) under RHC technique are presented in Fig. 15a for three different solution approaches (SAs). In SA 1, an initial solution is first found using the method described in II-B. Compared to SA 2, which solves the problem using proposed method

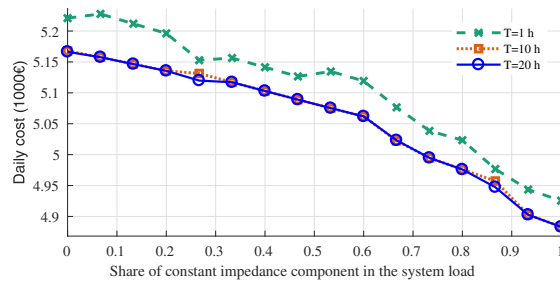
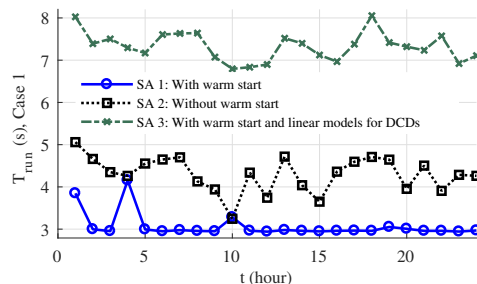
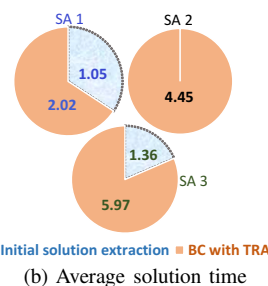


Fig. 14. System daily cost as a function of constant impedance share.



(a) Solution time for each scheduling window



(b) Average solution time

Fig. 15. Solution times in Case 1 with different solution approaches.

without this warm start, the solution time under SA 1 is almost always lower. By giving a warm start to the proposed solution method, the average reduction in solution time is more than 30 %. Instead of the perturbed models of DCDs in SA 1 and SA 2, SA 3 models these devices using a set of originally linear equations based on auxiliary binary variables (see subsection III-B). According to Fig. 15a, the solution time is always higher with SA 3, since the number of integer variables and branching burden are profoundly higher. Fig. 15b shows the average solution time for all SAs. Applying the proposed solution methodology (SA1), the solution times are quite acceptable. These study shows the performance of the proposed method and justified the application of the proposed BC-based solution methodology in terms of solution speed.

Concerning the solution speed, the performance of BC technique has been proven in the literature [27]. Moreover, the heuristic expediting techniques, such as the one introduced in subsection II-B, can be applied to find a tight upper bound on the problem objective function. These approaches are very effective in combination with BC technique, since they widely reduce the branching burden. This is the distinguished advantage of BC technique in terms of solution speed.

In terms of solution optimality, BC technique accurately deals with the problem discrete optimization variables. A TRA was adopted in this paper to solve the integer relaxed problems

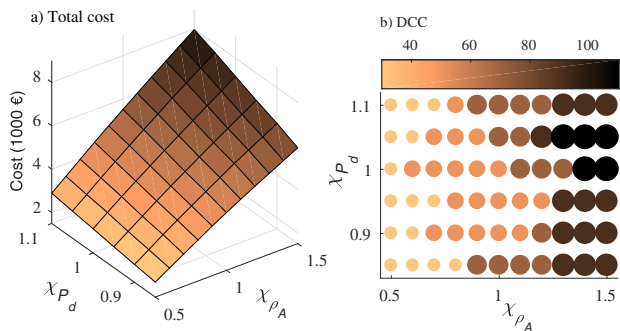


Fig. 16. a) Total daily cost and b) daily DCC.  $\chi_{\rho_A}$ : the scaling factor of hourly energy purchase prices.  $\chi_{P_d}$ : the scaling factor of power demands.

during the branching process. Byrd-Omojokun technique [2] was applied to cope with the inconsistency between the problem constraints and step-size constraints. It is the ability of TRAs to deal with this inconsistency that makes them globally convergent algorithms, compared to the other sequential approaches [2]. The performance of BC technique and the adopted TRA were theoretically analyzed in the literature. Here, the overall performance of the proposed methodology is analyzed based on the sensitivity studies conducted in this paper.

In cases 1-5, the results of applying the proposed scheduling algorithm for the different values of  $D_{OLTC}$ ,  $D_{CB}$  and  $T$  were presented. The sensitivity of the results to the change in these input parameters was analyzed. The rationales behind the variation in the optimal solution and the value of objective function due to the change in these parameters were presented. For all cases 1-5, the proposed method were applied 24 times to solve the DSP in 24  $T$ -hour scheduling windows. Each scheduling window has its own  $T$ -hour load and average energy purchase price profiles. The variations of the optimal solutions for successive scheduling windows were tracked and it was shown that these variations are rational and were expected. In subsection V-B, the sensitivity of the solution to the constant impedance coefficient of the load model was analyzed. The rationales behind the changes in the results were also presented.

Another sensitivity study is conducted here to analyze the changes of the optimal solution due to the change in the load levels and energy prices. The values  $\rho_A$  and load factor for all 24 hours (see Fig. 8 (a)) are multiplied by scaling factors  $\chi_{\rho_A}$  and  $\chi_{P_d}$ , respectively.  $\chi_{\rho_A}$  is changed from 0.5 to 1.5.  $\chi_{P_d}$  is changed from 0.85 to 1.1. The proposed algorithm is applied 24 times for each pair of  $\chi_{\rho_A}$ - $\chi_{P_d}$ , with  $D_{OLTC}=\text{€}20$ ,  $D_{CB}=\text{€}10$  and  $T=20$  h. Fig. 16 (a) shows as the scaling factors change, the total scheduling cost changes monotonically and smoothly. As  $\chi_{\rho_A}$  increases the total cost increases. The slope of such increase is always higher for the higher values of  $\chi_{P_d}$ . As  $\chi_{P_d}$  increases the total cost increases. The slope of such increase is always higher for the higher values of  $\chi_{\rho_A}$ . This is an indicator of the overall robustness of the algorithm. Fig. 16 (b) shows the BCCs in this study. The larger and darker circles indicate higher DCCs. According to 16 (b), as  $\chi_{\rho_A}$  increases, the DCC increases or does not change. The reason is that the higher energy prices justify more DCAs. As  $\chi_{P_d}$  changes, the DCC does not vary monotonically.

Despite the non-monotonic behavior of DCC, the total cost monotonically changes as discussed earlier. This best indicates the interactions between the DCAs, fast control actions and load level and confirms the results of cases 1-5. The results of cases 1-5, subsection V-B and this subsection indicate the robustness of the proposed scheduling algorithm against the variations of the problem input parameters.

## VI. CONCLUSIONS

The proposed solution methodology is able to solve the stochastic DSP within an acceptable solution time. The RHC technique is able to effectively co-optimize the operation of discrete and continuous control devices. With a short scheduling window ( $T$ ), the discrete control actions are not justified unless necessary. The scheduling algorithm cannot see the effects of DCAs in reducing the OC of the upcoming periods. Therefore, the DCAs might not be justified due to their higher cost. This results in the higher total costs. This means with a short SH it is not possible to exploit the voltage dependence nature of loads to reduce the system cost. With a proper tap-changing strategy in a longer scheduling window, lower costs can be achieved. The continuous control actions widely affect the required discrete control actions, and vice versa. It is imperative to simultaneously schedule these devices to take the interactions between these actions into account. This helps to avoid infeasible or sub-optimal solutions. It has also been observed that without updating the loads and upstream system models, the solution will be suboptimal or even infeasible. The originally linear models (based on auxiliary binary variables) for DCDs profoundly increase the solution time compared to the perturbed models. The reason is the huge branching burden required to handle these auxiliary binary variables.

To exploits the advantages of both short and long SHs, further studies are required to extend the proposed RHC-based scheduling algorithm. Similar to the operation of DCDs, the operation of storage systems and most demand response programs cannot be modeled within a short SH. The inclusion of the operation of storage systems and demand response programs in the proposed scheduling algorithm is suggested for future research activities on this topic.

## REFERENCES

- [1] Y. Xu, Z. Y. Dong, R. Zhang, and D. J. Hill, "Multi-timescale co-ordinated voltage/var control of high renewable-penetrated distribution systems," *IEEE Trans. Power Syst.*, vol. 32, no. 6, pp. 4398–4408, Nov 2017.
- [2] S. Bahrami and K. Amini, "An efficient two-step trust-region algorithm for exactly determined consistent systems of nonlinear equations," *J. Comput. Appl. Math.*, vol. 367, 2020.
- [3] W. Zheng, W. Wu, B. Zhang, and Y. Wang, "Robust reactive power optimisation and voltage control method for active distribution networks via dual time-scale coordination," *IET Gener. Transm. Distrib.*, vol. 11, no. 6, pp. 1461–1471, 2017.
- [4] A. OConnell, A. Soroudi, and A. Keane, "Distribution network operation under uncertainty using information gap decision theory," *IEEE Trans. Smart Grid*, vol. 9, no. 3, pp. 1848–1858, May 2018.
- [5] J. Ren, J. Hu, R. Deng, D. Zhang, Y. Zhang, and X. S. Shen, "Joint load scheduling and voltage regulation in the distribution system with renewable generators," *IEEE Trans Ind. Informat.*, vol. 14, no. 4, pp. 1564–1574, April 2018.

- [6] J. Robertson, G. P. Harrison, and A. R. Wallace, "A receding-horizon opf for active network management," in *22nd International Conference and Exhibition on Electricity Distribution (CIRED 2013)*, June 2013, pp. 1–4.
- [7] S. Moghadas and S. Kamalasadani, "Optimal fast control and scheduling of power distribution system using integrated receding horizon control and convex conic programming," *IEEE Trans. Ind. Appl.*, vol. 52, no. 3, pp. 2596–2606, May 2016.
- [8] A. Subramanian, M. Garcia, A. Domnguez-Garca, D. Callaway, K. Poolla, and P. Varaiya, "Real-time scheduling of deferrable electric loads," in *2012 American Control Conference (ACC)*, June 2012, pp. 3643–3650.
- [9] T. Khalili, A. Jafari, M. Abapour, and B. Mohammadi-Ivatloo, "Optimal battery technology selection and incentive-based demand response program utilization for reliability improvement of an insular microgrid," *Energy*, vol. 169, pp. 92 – 104, 2019 .
- [10] T. Khalili, S. Nojavan, and K. Zare, "Optimal performance of microgrid in the presence of demand response exchange: A stochastic multi-objective model," *Computers and Electrical Engineering*, vol. 74, pp. 429 – 450, 2019 .
- [11] T. Khalili, M. T. Hagh, S. G. Zadeh, and S. Maleki, "Optimal reliable and resilient construction of dynamic self-adequate multi-microgrids under large-scale events," *IET Renewable Power Generation*, vol. 13, no. 10, pp. 1750–1760, 2019 .
- [12] R. S. Ferreira, C. L. T. Borges, and M. V. F. Pereira, "A flexible mixed-integer linear programming approach to the ac optimal power flow in distribution systems," *IEEE Trans. Power Syst.*, vol. 29, no. 5, pp. 2447–2459, Sep. 2014.
- [13] B. A. Robbins, H. Zhu, and A. D. Domnguez-Garca, "Optimal tap setting of voltage regulation transformers in unbalanced distribution systems," *IEEE Trans. Power Syst.*, vol. 31, no. 1, pp. 256–267, Jan 2016.
- [14] Q. Li and V. Vittal, "Convex hull of the quadratic branch ac power flow equations and its application in radial distribution networks," *IEEE Trans. Power Syst.*, vol. 33, no. 1, pp. 839–850, Jan 2018.
- [15] S. R. Shukla, S. Paudyal, and M. Almassalkhi, "Efficient distribution system optimal power flow with discrete control of load tap changers," *IEEE Trans. Power Syst.*, vol. 34, no. 4, pp. 2970–2979, July 2019.
- [16] H. Gao, J. Liu, and L. Wang, "Robust coordinated optimization of active and reactive power in active distribution systems," *IEEE Trans. Smart Grid*, vol. 9, no. 5, pp. 4436–4447, Sep. 2018.
- [17] W. Wu, Z. Tian, and B. Zhang, "An exact linearization method for oltc of transformer in branch flow model," *IEEE Trans. Power Syst.*, vol. 32, no. 3, pp. 2475–2476, May 2017.
- [18] Y. Gu, H. Jiang, J. J. Zhang, Y. Zhang, H. Wu, and E. Muljadi, "Multi-timescale three-phase unbalanced distribution system operation with variable renewable generations," *IEEE Trans. Smart Grid*, vol. 10, no. 4, pp. 4497–4507, July 2019.
- [19] B. A. Robbins and A. D. Domnguez-Garca, "Optimal reactive power dispatch for voltage regulation in unbalanced distribution systems," *IEEE Trans. Power Syst.*, vol. 31, no. 4, pp. 2903–2913, July 2016.
- [20] D. Xu, Z. Chen, and L. Yang, "Scenario tree generation approaches using k-means and lp moment matching methods," *Journal of Computational and Applied Mathematics*, vol. 236, no. 17, pp. 4561 – 4579, 2012.
- [21] W. Sheng, K. Liu, and S. Cheng, "Optimal power flow algorithm and analysis in distribution system considering distributed generation," *IET Gener. Transm. Distrib.*, vol. 8, no. 2, pp. 261–272, February 2014.
- [22] A. Pouladi, A. K. Zadeh, and A. Nouri, "Control of parallel ultc transformers in active distribution systems," *IEEE Syst. J.*, to be published.
- [23] M. Bahadornejad and N. K. C. Nair, "Intelligent control of on-load tap changing transformer," *IEEE Trans. Smart Grid*, vol. 5, no. 5, pp. 2255–2263, Sept 2014.
- [24] M. Gheydi, A. Nouri, and N. Ghadimi, "Planning in microgrids with conservation of voltage reduction," *IEEE Syst. J.*, vol. 12, no. 3, pp. 2782–2790, Sep. 2018.
- [25] K. McKenna and A. Keane, "Open and closed-loop residential load models for assessment of conservation voltage reduction," *IEEE Trans. Power Syst.*, vol. 32, no. 4, pp. 2995–3005, July 2017.
- [26] K. Dehghanpour, Z. Wang, J. Wang, Y. Yuan, and F. Bu, "A survey on state estimation techniques and challenges in smart distribution systems," *IEEE Trans. Smart Grid*, vol. 10, no. 2, pp. 2312–2322, March 2019.
- [27] J. Kronqvist, D. E. Bernal, A. Lundell, and I. E. Grossmann, "A review and comparison of solvers for convex minlp," *Optimization and Engineering*, vol. 20, no. 2, pp. 397–455, Jun 2019 .

**Alireza Nouri (M17)** received the Ph.D. degree in electrical engineering from the Sharif University of Technology, Tehran, Iran, in 2016. He is now a senior power system researcher with the School of Electrical and Electronic Engineering, University College Dublin. His current research has been focused on power systems optimization and control.

**Alireza Soroudi (M13SM16)** received the Ph.D. degree in electrical engineering from the Grenoble-INP, Grenoble, France, in 2012. He is an Assistant Professor at UCD. His research interests include power systems planning and operation, risk, and uncertainty modeling.

**Andrew Keane (S04M07SM14)** received the Ph.D. degree in electrical engineering from the University College Dublin (UCD), Dublin, Ireland, in 2007. He is a Professor and Director of the Energy Institute at UCD. His research interests include power systems planning and operation, distributed energy resources, and distribution networks.